Infectious myonecrosis virus has a totivirus-like, 120-subunit capsid, but with fiber complexes at the fivefold axes

Jinghua Tang[a], Wendy F. Ochoa[a,1], Robert S. Sinkovits[a], Bonnie T. Poulos[b,2], Said A. Ghabrial[c], Donald V. Lightner[b,3], Timothy S. Baker[a,d,3], and Max L. Nibert[e,3]

[a]Department of Chemistry and Biochemistry and [d]Division of Biological Sciences, University of California at San Diego, La Jolla, CA 92093; [b]Aquaculture Pathology Laboratory, Department of Veterinary Science and Microbiology, University of Arizona, Tucson, AZ 85721; [c]Department of Plant Pathology, University of Kentucky, Lexington, KY 40546; and [e]Department of Microbiology and Molecular Genetics, Harvard Medical School, Boston, MA 02115

Edited by Reed B. Wickner, National Institutes of Health, Bethesda, MD, and approved September 18, 2008 (received for review July 11, 2008)

Infectious myonecrosis virus (IMNV) is an emerging pathogen of penaeid shrimp in global aquaculture. Tentatively assigned to family *Totiviridae*, it has a nonsegmented dsRNA genome of 7,560 bp and an isometric capsid of the 901-aa major capsid protein. We used electron cryomicroscopy and 3D image reconstruction to examine the IMNV virion at 8.0-Å resolution. Results reveal a totivirus-like, 120-subunit T = 1 capsid, 450 Å in diameter, but with fiber complexes protruding a further 80 Å at the fivefold axes. These protrusions likely mediate roles in the extracellular transmission and pathogenesis of IMNV, capabilities not shared by most other totiviruses. The IMNV structure is also notable in that the genome is centrally organized in five or six concentric shells. Within each of these shells, the densities alternate between a dodecahedral frame that connects the threefold axes vs. concentration around the fivefold axes, implying certain regularities in the RNA packing scheme.

dsRNA virus | electron cryomicroscopy | nonenveloped virus | penaeid shrimp | Totiviridae

Infectious myonecrosis virus (IMNV) was first isolated from whiteleg shrimp, *Litopenaeus vannamei,* from aquaculture farms in northeast Brazil (1, 2). The associated disease was characterized by skeletal muscle necrosis, most markedly in distal abdomen and tail, with mortality over the harvest cycle nearing 70%. Purified IMNV virions reproduce this disease in pathogen-free *L. vannamei* (2). Diagnostics are available using reverse transcription and PCR to distinguish IMNV from other RNA viruses of shrimp (3, 4), and a survey from Pernambuco, Brazil, detected IMNV in 9 of 11 farms (5). IMNV has also been detected in *L. vannamei* from Indonesian farms, probably after transfer of aquaculture stocks (4).

The genome sequence and many features of IMNV have been reported (2). Negatively stained virions exhibit an isometric capsid with a diameter of ≈400 Å. The virions contain a major capsid protein (MCP) of relative molecular weight (M_r) 106,000 and an N terminus of sequence IVSMENQSEID as shown by Edman degradation. The genome, a single molecule of 7,560-bp dsRNA, contains two extended ORFs in different frames of the plus strand: ORF1 in frame 1 (nucleotides 136-4953) and ORF2 in frame 3 (nucleotides 5241–7451). ORF1 encodes a 1,605-aa protein that includes the N-terminal sequence of the MCP starting at amino acid 705. The protein spanning amino acids 705-1605 have a sequence-predicted mass of 99 kDa, consistent with the M_r of the MCP. The MCP thus seems to be cleaved from a larger precursor. A 60-aa region at the N terminus of ORF1 shares sequence similarities with dsRNA-binding proteins. ORF2 encodes a 736-aa protein that contains typical motifs of an RNA-dependent RNA polymerase (RdRp). Proteins representing ORF2 and the first 704 aa of ORF1 have yet to be identified, although candidate minor proteins have been seen in denaturing gels of IMNV virions. Phylogenetic analyses link IMNV to members of the family *Totiviridae* of nonsegmented dsRNA viruses with isometric capsids, and most closely to Giardia lamblia virus (GLV) (2, 6). IMNV would be the first member of this family to infect a host other than a fungus or a protozoan (7).

Further examination of the IMNV sequence has revealed other features (8). These include (*i*) two encoded "2A-like" peptide motifs (9), which specify a cotranslational autolytic or termination-reinitiation mechanism and are thus likely involved in ORF1 polyprotein "cleavage" into three products (the C-terminal of which includes the MCP); (*ii*) a 199-nt overlap between the end of ORF1 in frame 1 and the start of ORF2 in frame 3; and (*iii*) a "shifty heptamer" motif (10) and predicted RNA pseudoknot (11) in the region of ORF1-ORF2 overlap, specifying ORF2 to be translated as a fusion with ORF1 by −1 ribosomal frameshifting. Features *ii* and *iii* bring the predicted ORF2 coding strategy more in line with those of GLV (6) and several other members of family *Totiviridae*, including Saccharomyces cerevisiae virus L-A (ScV-L-A) (12). The 1,734-aa MCP/RdRp fusion is expected to assemble in only a few copies per IMNV virion, with the MCP region occupying a position in the capsid and the RdRp region projecting into the interior, where it can function in transcription as discussed for ScV-L-A (13, 14). Some of the N-terminal fragments of IMNV ORF1 might also be assembled into virions. Function of the IMNV-encoded 2A-like motifs at polyprotein cleavage has been demonstrated (15).

Most members of family *Totiviridae* lack the means to be transmitted through extracellular media as part of their natural life cycles (7). Instead, they are passed only vertically at cell division or horizontally by hyphal anastomosis. Exceptions to date comprise only GLV and the tentative totivirus IMNV. In addition, IMNV is the only one of these viruses that is known to cause a host disease.

Scrutiny of electron micrographs from Poulos *et al.* (2) suggested that fiber-like densities may extend from IMNV virions, a novel feature for family *Totiviridae*. To investigate this possibility, we undertook transmission electron cryomicroscopy (cryoTEM) and 3D image reconstruction. Results at 8.0-Å resolution reveal a totivirus-like, 120-subunit capsid, 450 Å in diameter but with fiber complexes protruding a further 80 Å at the fivefold (5f) axes. These

Author contributions: J.T., W.F.O., R.S.S., B.T.P., D.V.L., T.S.B., and M.L.N. designed research; J.T., W.F.O., R.S.S., B.T.P., D.V.L., T.S.B., and M.L.N. performed research; J.T., R.S.S., B.T.P., D.V.L., and T.S.B. contributed new reagents/analytic tools; J.T., W.F.O., R.S.S., B.T.P., S.A.G., D.V.L., T.S.B., and M.L.N. analyzed data; and J.T., R.S.S., S.A.G., D.V.L., T.S.B., and M.L.N. wrote the paper.

The authors declare no conflict of interest.

This article is a PNAS Direct Submission.

[1]Present address: Electron Microscopy Facility, Burnham Institute for Medical Research, La Jolla, CA 92037.

[2]Present address: Marine Phage Laboratory, Department of Ecology and Evolutionary Biology, University of Arizona, Tucson, AZ 85721

[3]To whom correspondence may be addressed. E-mail: dvl@u.arizona.edu, tsb@ucsd.edu, or mnibert@hms.harvard.edu.

This article contains supporting information online at www.pnas.org/cgi/content/full/0806724105/DCSupplemental.

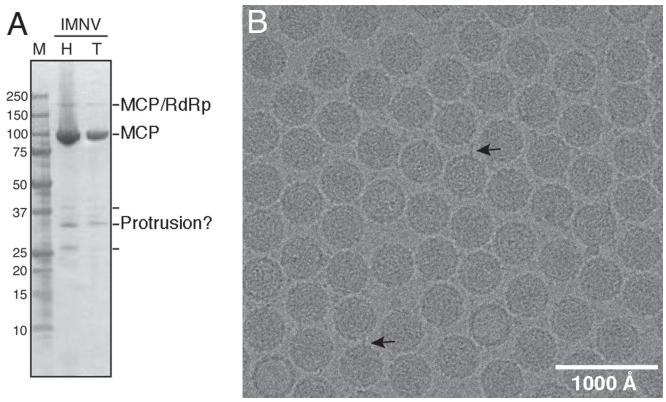

Fig. 1. Preparation of IMNV virions. (*A*) Denaturing polyacrylamide gel of purified virions. M, molecular weight markers (values in kDa at *Left*); H, purified virions prepared from shrimp heads; T, purified virions prepared from shrimp tails. (*B*) Unprocessed cryomicrograph of IMNV virions purified from shrimp heads. Arrows, examples of surface protrusions; many others are evident throughout the micrograph.

protrusions likely mediate roles in the extracellular transmission and pathogenesis of IMNV. Additionally, the virion interior contains five or six concentric shells of density attributed to the genome. Within each of these shells, the densities alternate between a dodecahedral frame that connects the threefold (3f) axes vs. concentration around the 5f axes, implying certain regularities in the RNA packing scheme.

Results

Preparation of Virions. Virus particles were purified from heads or tails (see *Materials and Methods*) of IMNV-infected *L. vannamei*, using a modification of described protocols including serial centrifugations in sucrose and CsCl gradients (2). Estimated concentrations of the purified particles were 2–6 mg/ml.

Denaturing polyacrylamide gels of the purified virions (Fig. 1*A*) confirmed the MCP as the major protein component, with M_r near 100,000 (predicted mass, 99 kDa). A minor protein with M_r near 200,000 likely corresponds to the MCP/RdRp fusion (predicted mass, 196 kDa). Three or four other minor proteins with M_r values in the 20,000–40,000 range are also visible in the gel, as has been previously noted (2), and may correspond to one or more of the N-terminal fragments of ORF1.

Negative-stain electron microscopy was performed to ascertain quality of the purified preparations. As expected, virus particles from shrimp heads and tails appeared very similar: well dispersed and consistently sized, with mostly unbroken capsids that excluded stain (data not shown). Particles vitrified and visualized by cryoTEM also appeared well preserved, with consistent size, shape, and density (Fig. 1*B*). Closer inspection suggested the presence of 50- to 100-Å protrusions widely spaced on the surfaces of most particles (Fig. 1*B*, arrows).

3D Structure of the Virion. A 3D reconstruction of IMNV virions from shrimp tails was computed from 5,629 particle images. The estimated resolution was 8.0 Å [supporting information (SI) Fig. S1], based on a Fourier-shell correlation threshold of 0.5 (16). A 3D reconstruction of IMNV virions from shrimp heads was computed to a similar resolution and yielded essentially identical conclusions (unpublished data).

Overall features of the IMNV virion were revealed in a central section of the 3D map (Fig. 2*A*). The virion contains a single-layered capsid, with a maximum thickness of ≈50 Å (median, ≈30 Å) and an outer diameter of ≈450 Å. The capsid exhibits respectively coarse and smooth outer and inner surfaces. Both punctate and linear densities suggestive of secondary-structure elements are

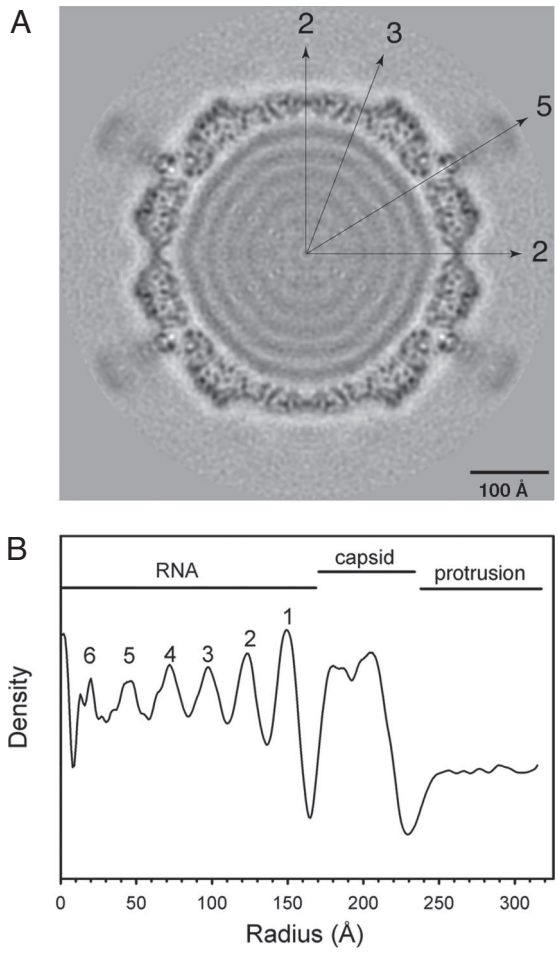

Fig. 2. 3D reconstruction of IMNV virion at 8.0-Å resolution. (*A*) Central section, with density values coded in grayscale (darker, denser). Symmetry axes are labeled in the upper right quadrant. (*B*) Radial density plot. Evident layers are labeled at top.

visible within the capsid. Across much of the capsid, there appears to be a greater concentration of density near the outer and inner surfaces, with an area of lower density between, and this appearance is supported by a radial density plot showing a double peak in the capsid region (Fig. 2*B*).

Consistent with the protrusions seen in micrographs, additional densities are evident in the central section, extending ≈80 Å beyond the capsid at the 5f axes (Fig. 2*A*). These elements have lower density and resolution than the capsid, which might be explained by their (*i*) lateral flexibility, (*ii*) less than full occupancy of the 12 5f sites, and/or (*iii*) smearing due to 5f averaging of a nonpentameric structure. A space-filling surface view shows the protrusions to be complex fiber-like elements (Fig. 3*A*). The fibers comprise at least three morphologic domains: an outer knob; a middle stalk; and an inner, capsid-anchored foot (Fig. 3*B*). The total length of each protrusion, including the foot, is ≈100 Å.

Interior to the capsid, other lower-resolution densities are visible as five or six concentric rings (Figs. 2*A* and 4*A*), typical of the packaged genome in many dsRNA viruses. These rings are also visible as peaks in the radial plot (Fig. 2*B*). The average spacing between density peaks is ≈26 Å, similar to that in orthoreovirus (≈26 Å) (17) but less than that in ScV-L-A (≈30 Å) (18). The layers of RNA in IMNV virions do not appear to be perfectly spherical; instead, bulges are seen at the icosahedral twofold (2f) axes and flattenings near the 5f axes (Figs. 2*A* and 4*A*). These features led us to examine the RNA organization in more detail. Density-coded

MICROBIOLOGY

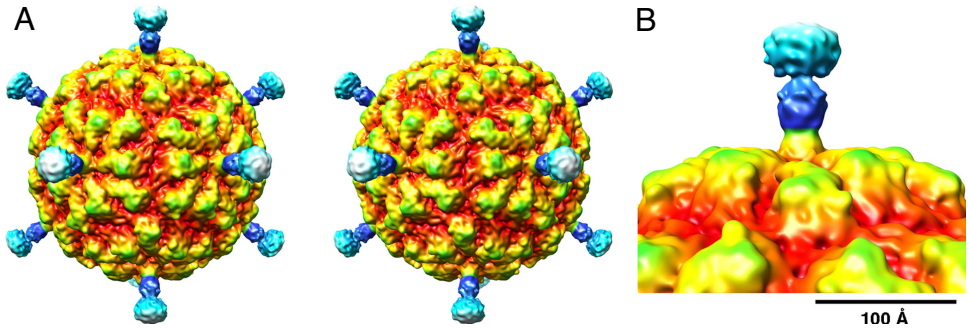

Fig. 3. Fiber-like protrusions at 5f axes of IMNV virion. (*A*) Radially color-coded surface view of IMNV virion, in stereo, with complex protrusions evident at the 5f axes. (*B*) Close-up view of one protrusion and the surrounding capsid. The 3D map was calculated at 10-Å resolution for this figure, with the lowest-resolution Fourier components amplified to enhance low-density features (see *Materials and Methods*).

spherical sections at single radii identify sublayers in which the densities span between the 3f axes, forming a dodecahedral frame (Fig. 4 *B* and *E* and data not shown), closely alternating with sublayers in which the densities concentrate around the 5f axes (Fig. 4 *C* and *F* and data not shown). This interpretation is reinforced by space-filling surface views of the two outer shells of RNA (Fig. 4 *D* and *G*). These close alternations in density positionings between sublayers are easy to see in a movie (Movie S1) and imply certain regularities in the RNA packing scheme.

Organization of the Capsid. When highlighted by a color-coded surface view (Fig. 5*A*), the IMNV capsid is seen to be a 120-subunit T = 1, or so-called "T = 2" (19), icosahedron. As in all such capsids, there are 60 copies each of two chemically identical subunits, MCP-A and -B, distinguished by their nonequivalent positions (Fig. 5 *A* and *C*). The A subunits form pentameric clusters around each of the 12 5f axes, and the B subunits form trimeric clusters around each of the 20 3f axes. Moreover, five B subunits lie in a staggered arrangement around each A pentamer so that together they form a compact decamer centered at each 5f axis. The A subunits within each decamer participate in 5f-symmetric interactions, whereas all other A:B contacts within each decamer are asymmetric. In IMNV, interactions between decamers mostly occur in two ways: (*i*) two A subunits, one from each decamer in an adjacent pair, participate in 2f-symmetric contacts across each icosahedral 2f axis (Fig. 5*C*, blue and cyan), and (*ii*) three B subunits, one from each of three adjacent decamers, participate in 3f-symmetric interactions around each 3f axis (Fig. 5 *A* and *C*). These interdecamer interactions, including the 2f-symmetric A:A contacts across each 2f axis, are broadly similar to those in ScV-L-A (Fig. 5*B*).

The asymmetric unit of the icosahedron, 60 of which form the capsid, includes a single MCP-A/B pair. There are quasi-2f-symmetric interactions between A and B subunits from adjacent decamers (Fig. 5*C*, blue and pink, also cyan and orange), which allow the capsid to be built from 60 such dimers. However, the A:B contacts within these quasisymmetric dimers are relatively limited in terms of the buried surface areas. More extensive contacts occur between each asymmetric pair of A and B subunits within each decamer (Fig. 5*C*), favoring one of these asymmetric A/B dimers to be chosen as the icosahedral asymmetric unit. There are in fact two choices for how to pair A and B subunits in an asymmetric dimer, one in which the two subunits are less parallel to each other (Fig. 5*C*, blue and red vs. blue and orange). In ScV-L-A (Fig. 5*B*), the more and less parallel A/B dimers have been variably designated as the asymmetric unit (14, 20), and in IMNV the choice seems to be similarly arbitrary (Fig. 5*C*). Which, if any, of these different types of A/B dimer may serve as an assembly intermediate remains to be determined.

Although the interdecamer A:A, B:B, and A:B interactions in IMNV are broadly similar to those in ScV-L-A, there are some differences. In ScV-L-A the long axes of the A and B subunits point tangentially to the 2f and 3f icosahedral axes, respectively (Fig. 5*B*). In IMNV, conversely, these subunit axes appear to point more directly toward the respective symmetry axes (Fig. 5*A*). Both of these differences may contribute to expanding the IMNV capsid, giving it a more spherical outline than ScV-L-A.

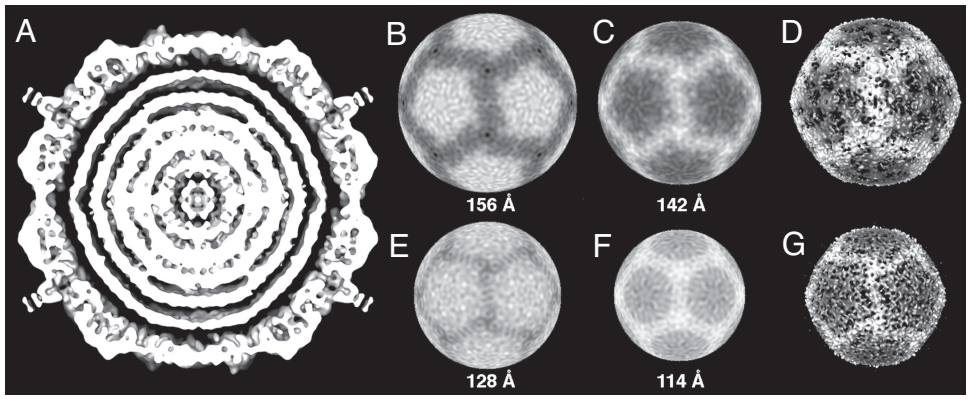

Fig. 4. RNA densities in interior of IMNV virion. (*A*) Central section of space-filling model, with front half of particle removed. (*B*, *C*, *E*, *F*) Spherical sections through the two outermost shells of RNA, at single radii as indicated below each image, with density values coded in grayscale (darker, denser). Radii at which the densities define a dodecahedral frame connecting the 3f axes (*B* and *E*) closely alternate with other radii at which the densities concentrate around the 5f axes (*C* and *F*). (*D* and *G*) Space-filling surface views of the two outermost shells of RNA. To obtain these views, densities were zeroed above radius 164 Å (*D*) or 137 Å (*G*). The 3D map used for Fig. 3 was also used for this figure.

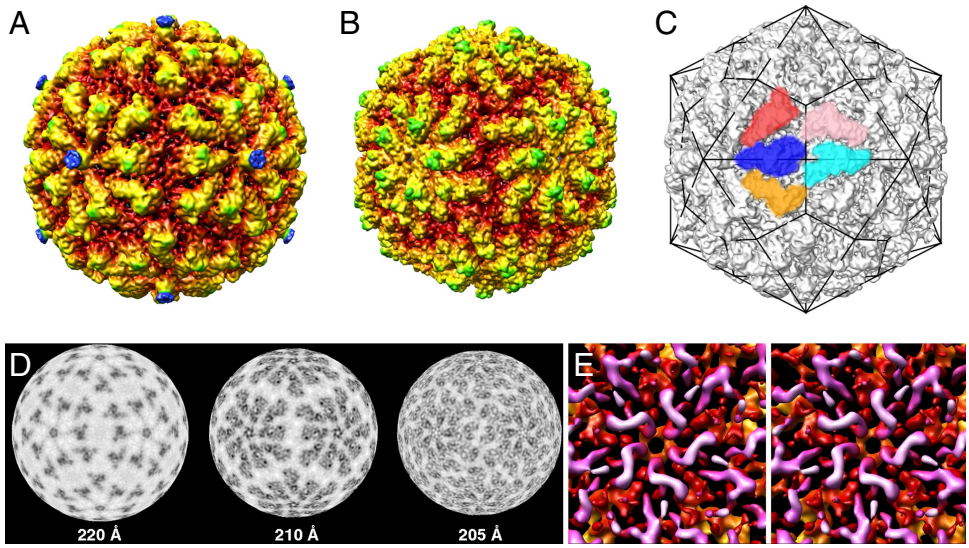

Fig. 5. IMNV capsid at 8.0-Å resolution and comparison with X-ray model of ScV-L-A capsid computed to 8.0-Å resolution. (*A*) Radially color-coded surface view of IMNV virion, with outer parts of protrusions removed by zeroing densities above radius 225 Å. (*B*) Comparable surface view of ScV-L-A (14) to which the same radial color table was applied. (*C*) Surface view of IMNV virion in black and white, with overlay of T = 1 model and selected MCP-A subunits (blue, cyan) and -B subunits (red, pink, orange) highlighted for reference in text. (*D*) Spherical sections at different radii as indicated below each image, with density values coded in grayscale (darker, denser). (*E*) Space-filling slab view, in stereo, as seen from the inner surface of the IMNV capsid. Tube-like densities (lavender) that form two concentric rings around the 5f axis (inner and outer rings from MCP-A and -B subunits, respectively) are interpreted as α helices.

Further Details of the Capsid and Subunits. The outer surface of the IMNV capsid consists of 12 pentagon-shaped regions demarcated by wide canyons that run between adjacent 3f axes and reach their deepest points near the 2f axes (Fig. 5*A*). Each pentagon has a small, central knob attributed largely to the fiber foot, surrounded by two sets of five mesas (raised regions with relatively flat tops) and 10 narrow canyons that separate the mesas (Fig. 5*A*; also see Fig. 5*D*). The MCP-A and -B subunits form mesas with similar morphologies and lie closest to and farthest from the 5f axes, respectively. Similar, yet straighter and less massive mesas are seen in ScV-L-A (Fig. 5*B*). No pores that fully span the capsid are evident in IMNV.

Comparable densities to the 5f-centered surface knob in IMNV are not seen in ScV-L-A (Fig. 5*B*), which lacks fiber complexes. Instead, in ScV-L-A there is a capsid-spanning pore at the 5f axis. In IMNV the fiber foot does not seem to penetrate the capsid, but only anchors atop it. By binding in that position, the foot obscures a capsid-spanning pore at the 5f axis that is otherwise also present in IMNV. Aside from the fiber complexes, other capsid densities can be attributed to MCP-A or -B; thus, we consider it unlikely that N-terminal fragments of IMNV ORF1 contribute to other features.

Density-coded spherical sections (Fig. 5*D*) corroborate the totivirus-like capsid organization described above. At high radii, the molecular outlines of MCP-A and -B are well separated (Fig. 5*D*, 220 Å), but numerous intersubunit contacts are evident at lower radii (Fig. 5*D*, 210 and 205 Å). Intradecamer associations seem to involve 5f A:A and asymmetric, lateral A:B contacts. Interdecamer associations seem to involve 3f B:B and 2f A:A contacts as well as more limited, quasi-2f-symmetric A:B contacts.

Both punctate and linear features consistent with secondary-structure elements are visible in spherical sections through the capsid (Fig. 5*D*). The number of such features especially suggestive of α helices is consistent with secondary-structure predictions, indicating a reasonably high α-helical content for the IMNV MCP (data not shown), as known for the "T = 2" proteins of other dsRNA viruses, including ScV-L-A (14, 17, 19, 21, 22). Tube-like densities interpreted as α helices are also visible in slab views of the IMNV capsid (Fig. 5*E*). Detailed comparisons between the coat protein folds of IMNV and ScV-L-A await higher-resolution analyses of IMNV.

Although occupying nonequivalent capsid positions, MCP-A and -B have similar structures, as reflected by not only their molecular outlines but also their patterns of densities reflecting the protein folds. For example, a putative α-helix in cross-section is similarly positioned near the 5f-distal end of each at radius 210 Å (Fig. 5*D*). In most cases, the shared features of MCP-A and -B are found at slightly different radii (higher in A than in B), relating to their nonequivalent positions and necessitating comparisons across radii to recognize their full likenesses. With complete protein folds from future analyses, nonetheless, we expect to see differences in the A and B subunits, especially near regions of contact. One such region in which A/B differences appear present in the 8.0-Å map is at the 5f-proximal tips of the subunits. In B there is a looped structure at this tip, whereas in A the loop appears to have swung open so that it reaches toward the 5f axis, providing contact with the fiber foot (Fig. 5*D*, 210 Å, and Fig. S2).

Discussion

Protrusions. IMNV possesses a 120-subunit T = 1 (so-called "T = 2") capsid to which fiber complexes are directly anchored. Others of these capsids, unique to dsRNA viruses in nature, are either unadorned (family *Partitiviridae* and other members of family *Totiviridae*) (14, 22–24) or coated with one or more additional, often T = 13, protein layer(s) (families *Cystoviridae* and *Reoviridae*) (19, 21, 25). In certain members of family *Reoviridae*, fibers are then anchored to the outer, T = 13 layer(s), for example, at the 5f axes in orthoreoviruses (25).

On the basis of surface fibers in other viruses, the IMNV protrusions are almost certainly involved in cell entry, including receptor binding and/or membrane penetration. Their presence correlates with the fact that IMNV is nearly unique in family *Totiviridae* in being transmitted extracellularly between host organisms (2, 7). It is possible that the MCP of IMNV has also evolved to share roles in cell entry with the fiber complexes. Other members of family *Totiviridae* are associated with latent, avirulent infections of their hosts (7). Conversely, IMNV is associated with an often fatal disease in penaeid shrimp (1, 2). We thus propose that the IMNV protrusions also contribute to its virulence and specific patterns of pathogenesis.

The IMNV structure suggests a simple evolutionary mechanism—adorn the capsid with fibers—for providing a new set of functions that expands the infectivity capabilities of a virus. Evolution of IMNV from simpler totiviruses may have included acquisition of fiber-coding sequences to allow extracellular transmission. But from where were the fiber sequences acquired? Clues in answer to this question have not been apparent from database homology searches (ref. 2 and data not shown). As for how these new sequences are positioned in the IMNV genome to allow for expression, incorporation of "2A-like" sequences to provide cotranslational polyprotein processing (9) has served as an elegant solution (2, 8, 15). Alternatively, the IMNV genome organization may have been ancestral, with the fiber sequences lost from simpler totiviruses during adaptation to hosts in which extracellular transmission does not occur.

The precise morphology and structure of the IMNV protrusions remain to be determined. In the present study 5f symmetry was imposed on them by the reconstruction process, but they seem unlikely to be pentamers. On the basis of better-characterized fibers, such as that of orthoreoviruses (26), the IMNV protrusions seem more likely to be trimers. The resulting symmetry mismatch (trimer complex at 5f axis) is not uncommon in the virus world and may promote shedding of the fibers during cell entry (see below).

Which of the three N-terminal peptides of IMNV ORF1 (2, 8, 15) forms the fiber complexes? Because peptide (pep)1, the 10-kDa dsRNA-binding protein homologue, probably plays a role in modulating innate immunity after expression in infected cells, it seems unlikely to be part of the protrusions. Pep2 (32 kDa) or pep3 (38 kDa) thus seems more likely. By defining the structural envelope of one fiber complex from the 3D map, we estimated its molecular mass to be ≈90 kDa. Because the mass of a pep2 or pep3 trimer would approximate 95 or 115 kDa, respectively, each of these remains a candidate. Fibrous regions of viral surface proteins can include α-helical coiled coils (27); however, none of the IMNV proteins have predicted coiled-coil motifs (groups.csail.mit.edu/cb/paircoil2). On the other hand, a neighboring pair of long regions without charged residues in the N-terminal half of pep2 (Fig. S3) may suggest a role in membrane penetration. One of these regions, amino acids 42–62, receives a significant score for membrane-spanning potential (www.ch.embnet.org/software/TMPRED_form.html).

Capsid. Despite little or no clear sequence homology in their coat proteins, the organization of the IMNV capsid is very similar to that of prototype totivirus ScV-L-A (14, 20, 23), including that MCP-A subunits from adjacent A/B decamers appear to make 2f-symmetric contacts across the icosahedral 2f axes and to "seal off" this axis from the MCP-B subunits. The latter arrangement is also like that in members of family *Reoviridae* (17, 19) but appears to be unlike that in members of families *Cystoviridae* and *Partitiviridae*, where B subunits from adjacent decamers appear to make 2f-symmetric contacts across the icosahedral 2f axes (21, 22). Of note, the IMNV capsid is less perforated than the ScV-L-A capsid (14, 18, 20, 23) (see Fig. 5 *A* and *B*), perhaps representing an adaptation to the rigors of extracellular transmission. The IMNV MCP is larger than the ScV-L-A coat (Gag) protein (901 aa vs. 680 aa), which may help it to form a more contiguous shell.

A fascinating feature of the ScV-L-A capsid is that it cleaves the 5′ caps from yeast mRNAs, facilitating translation of its own uncapped transcripts (14, 18). Decapping is mediated by a surface-exposed "trench" in the ScV-L-A coat protein, located at the 5f-distal end of each A and B subunit. There is no biochemical evidence that IMNV uses decapping of shrimp mRNAs as a strategy to facilitate its own translation, and although the current 3D map is insufficient to address this question definitively, we see no clear evidence for the presence of such a trench in IMNV.

RNA. The IMNV genome (7,560 bp) (2) is ≈65% larger than that of ScV-L-A (4,579 bp) (12), but the IMNV capsid diameter (450 Å) (see Fig. 2 *A* and *B*) is <3% larger than that of ScV-L-A (440 Å). In fact, the estimated volume of the IMNV interior (1.85×10^7 Å^3) is ≈9% larger than that of ScV-L-A (1.72×10^7 Å^3). Moreover, the IMNV genome is more tightly packed (spacing of density peaks, ≈26 Å) (see Fig. 2 *A* and *B*) than that of ScV-L-A (≈30 Å) (18). Thus, ScV-L-A is less fully filled than IMNV, which is filled to a similar extent as orthoreoviruses (17).

The pattern of densities in the IMNV interior, alternating in closely spaced sublayers between a dodecahedral frame connecting the 3f axes vs. concentration around the 5f axes, is intriguing. This pattern is remarkably similar to that of the single-stranded RNA genome of nodaviruses (28, 29), except that in IMNV the pattern extends over multiple layers. In nodaviruses the pattern is proposed to reflect RNA-capsid interactions that promote both short- and long-range base pairing within the genome, resulting in a complex RNA path dominated by formation of duplex stems that interact with the capsid along the edges of the dodecahedron. In IMNV, however, because the genome is already dsRNA, this explanation seems unlikely. Rather, the pattern in IMNV seems more likely to reflect certain regularities in the scheme for dsRNA winding within the interior, in which the outer layer of dsRNA is directed by interactions with the capsid to bind preferentially along the edges of the dodecahedron. Repetition of this pattern in the inner layers may then be determined by this directed pattern in the outer layer. The presence of the RdRp (as part of the MCP/RdRp fusion) projecting into the interior in IMNV may also contribute to this pattern by anchoring at least one end of the dsRNA and by directing its path, by either binding or steric exclusion, at other points in the winding scheme.

Like those of other dsRNA viruses, the IMNV particle would be expected to enter the cytoplasm as the outcome of cell entry, where it would transcribe and export copies of the viral mRNA(s) for translation by host ribosomes (30). But where is the capsid-spanning pore through which these mRNAs are exported and/or substrate nucleotides imported? The only notable pores through the IMNV capsid are at the 5f axes, and those are covered by the protrusions. One possibility is that the 5f axis near which the MCP/RdRp subunit is incorporated is not competent to anchor a protrusion so that that pore is constitutively open. Another possibility is that the protrusions are lost during or after cell entry and that the pores are thereby uncovered for transcript release and nucleotide import. A similar step is known for orthoreovirus (25, 31). Indeed, fiber loss may be an essential part of the cell entry mechanism of IMNV.

Taxonomy. IMNV shares prime similarities with members of family *Totiviridae*. It has a nonsegmented dsRNA genome and seems to use −1 ribosomal frameshifting to express its RdRp in fusion with the MCP. It clusters with this family in sequence-based phylogenetic comparisons, albeit distantly, and its closest relative is GLV (prototype of genus *Giardiavirus*). From the present results, we also know that its capsid is organized much like that of ScV-L-A (prototype of genus *Totivirus*) as well as those of two other family members, Ustilago maydis virus P4 and Helminthosporium victoriae 190S virus (23, 24), for which 3D structures are known. Its dissimilarities are also important and include infection of a crustacean arthropod host; a larger genome, with coding capacity beyond MCP and RdRp; fiber-like protrusions on the virion surface; capability to transmit extracellularly, like GLV; and association with host disease. On the basis of these facts, we consider it reasonable to propose a new monotypic genus to accommodate IMNV but to retain this genus in family *Totiviridae*. As other viruses related to IMNV are discovered, however, one might then argue to separate those into a new family of phylogenetically distinct, nonsegmented dsRNA viruses that possess, in at least some cases, the machinery for extracellular transmission.

Materials and Methods

Virion Purification. Virions were purified from IMNV-infected *L. vannamei* by a procedure modified from Poulos *et al.* (2). Gnathothoraces (''heads'') and tail muscles (''tails'') from 30 subadult shrimp were treated separately in an effort to optimize yields and purity from either portion. There is no evidence that virions isolated from heads or tails are different, and preparations from each have been used to induce IMNV infection in the lab. Tissues were homogenized in 20 mM Tris/HCl (pH 7.5), 400 mM NaCl (TN buffer), and large debris were removed by centrifugation at 8,000 $\times$ *g*. After centrifugation for 3 h at 205,000 $\times$ *g*, the pellets were resuspended in TN buffer. Lipids were removed with Freon (heads) or fumed silica (tails), and the suspensions were mixed with 1 g charcoal for 10 min. Charcoal was removed with Celite 535. After pelleting as above, the pellets were again resuspended in TN buffer, layered onto a 15–40% (wt/wt) sucrose gradient, and centrifuged for 2 h at 286,000 $\times$ *g*. Peak fractions in the lower third of the gradient were collected and washed with TN buffer. The peak suspension from tails was treated on a second such sucrose gradient for further purification. A 20–50% (wt/wt) CsCl gradient was used for final purification. This gradient was centrifuged for 16 h at 136,000 $\times$ *g*, the peak fractions were collected and washed, and pellets were resuspended in TN buffer. The purified virions were subjected to denaturing polyacrylamide gel electrophoresis followed by staining with Coomassie blue. They were also negatively stained with 2% phosphotungstic acid and examined using a Philips CM12 microscope.

CryoTEM. Small (3-μl) aliquots of purified virions from shrimp tails ($\approx$2.5 mg/ml) were vitrified for cryoTEM via standard, rapid freeze-plunging procedures (32). Samples were applied to Quantifoil holey grids that had been plasma-cleaned for 25 sec in an E.A. Fischione 1020 unit. Grids were then transferred into a precooled Gatan 626 cryotransfer holder, which maintained the specimen at liquid-nitrogen temperature in the FEI Sphera microscope. Micrographs were recorded on Kodak SO-163 electron-image film at 200 keV under low-dose conditions ($\approx$15 e/Å^2) and at a nominal magnification of $\times$50,000.

3D Reconstruction. Twenty-four micrographs, exhibiting minimal specimen drift and image astigmatism and recorded at underfocus settings of between 0.7 and 2.0 μm, were digitized on a Zeiss scanner at 7-μm intervals representing 1.4-Å pixels at the specimen. RobEM (cryoem.ucsd.edu/programDocs/runRobem.txt) was used to extract individual particle images, each 449 $\times$ 449 pixels in size, and to preprocess them as described (32). Processing began with a 15-Å map of head-derived virions, which had been generated earlier in the study (unpublished data). This map served as a starting model to initiate full orientation and origin determinations of the full set of 5,629 particle images of tail-derived virions by using the current version of AUTO3DEM (33). The result was a 3D reconstruction at 12-Å resolution after five iterative cycles. Several cycles of orientation and origin refinement with the PO^{2}R and P3DR functions of AUTO3DEM then enabled us to improve the resolution to 8.0 Å. Effects of the microscope contrast-transfer function were compensated in part by inverting image phases in spatial frequency bands where contrast reversals occurred (34). To enhance the lowest-resolution features of protrusions and RNA, another 3D map, at 10-Å resolution, was calculated in which spatial frequency components up to the first peak in the contrast-transfer function for each image were amplified using $\delta 1 = 0.4$ (35). Graphics were generated with RobEM and Chimera (36). Contour levels were adjusted to optimize relevant features for each figure: 0.6 σ for Fig. 3; 2.0 σ for Fig. 4 *A*, *D*, and *G*; 1.5 σ for Fig. 5 *A*-*C*; and 3.0 σ for Fig. 5*E*. Handedness was assigned to match that of ScV-L-A (14).

ACKNOWLEDGMENTS. We thank N. Olson for help with microscopy, A. Rusnak for preliminary analyses of head-prep images, and K. Chang and S. Dunn for scanning of tail-prep images. This work was supported in part by National Institutes of Health (NIH) Grants R37 GM033050 (to T.S.B.) and R01 AI46440 (to M.L.N.) plus U.S. Department of Agriculture Grants NRICRP 2001-35319-10010 (to S.A.G.) and CSREES 2004-38808-02142 (to D.V.L.). The San Diego Supercomputer Center provided partial support for R.S.S. and for access to TeraGrid computing. Shared NIH instrumentation grant 1S10 RR020016-01 as well as support from the University of California-San Diego and the Agouron Foundation (all to T.S.B.) were used to establish the cryoTEM facilities used in this study.

1. Lightner DV, *et al.* (2004) Infectious myonecrosis: new disease in Pacific white shrimp. *Glob Aquac Advocate* 7:85.
2. Poulos BT, Tang KF, Pantoja CR, Bonami JR, Lightner DV (2006) Purification and characterization of infectious myonecrosis virus of penaeid shrimp. *J Gen Virol* 87:987–996.
3. Andrade TPD, Srisuvan T, Tang KFJ, Lightner DV (2007) Real-time reverse transcription polymerase chain reaction assay using TaqMan probe for detection and quantification of infectious myonecrosis virus (IMNV) *Aquaculture* 264:9–15.
4. Senapin S, Phewsaiya K, Briggs M, Flegel TW (2007) Outbreaks of infectious myonecrosis virus (IMNV) in Indonesia confirmed by genome sequencing and use of an alternative RT-PCR detection method. *Aquaculture* 266:32–38.
5. Pinheiro ACAS, *et al.* (2007) Epidemiological status of Taura syndrome and infectious myonecrosis viruses in *Penaeus vannamei* reared in Pernambuco (Brazil). *Aquaculture* 262:17–22.
6. Wang AL, Yang HM, Shen K, Wang CC (1993) Giardiavirus double-stranded RNA genome encodes a capsid polypeptide and a gag-pol-like fusion protein by a translational frameshift. *Proc Natl Acad Sci USA* 90:8595–8599.
7. Ghabrial SA (2008) Totiviruses. *Encyclopedia of Virology*, eds Mahy B, van Regenmortel MHV (Elsevier/Academic, London), 3rd Ed pp 163–174.
8. Nibert ML (2007) '2A-like' and 'shifty heptamer' motifs in penaeid shrimp infectious myonecrosis virus, a monosegmented double-stranded RNA virus. *J Gen Virol* 88:1315–1318.
9. Donnelly ML, *et al.* (2001) The 'cleavage' activities of foot-and-mouth disease virus 2A site-directed mutants and naturally occurring '2A-like''sequences. *J Gen Virol* 82:1027–1041.
10. Bekaert M, *et al.* (2003) Towards a computational model for -1 eukaryotic frameshifting sites. *Bioinformatics* 19:327–335.
11. Plant EP, *et al.* (2003) The 9-Å solution: How mRNA pseudoknots promote efficient programmed -1 ribosomal frameshifting. *RNA* 9:168–174.
12. Icho T, Wickner RB (1989) The double-stranded RNA genome of yeast virus L-A encodes its own putative RNA polymerase by fusing two open reading frames. *J Biol Chem* 264:6716–6723.
13. Ribas JC, Wickner RB (1998) The Gag domain of the Gag-Pol fusion protein directs incorporation into the L-A double-stranded RNA viral particles in *Saccharomyces cerevisiae*. *J Biol Chem* 273:9306–9311.
14. Naitow H, Tang J, Canady M, Wickner RB, Johnson JE (2002) L-A virus at 3.4 Å resolution reveals particle architecture and mRNA decapping mechanism. *Nat Struct Biol* 9:725–728.
15. Luke GA, *et al.* (2008) Occurrence, function and evolutionary origins of '2A-like' sequences in virus genomes. *J Gen Virol* 89:1036–1042.
16. Harauz G, van Heel M (1986) Exact filters for general geometry three dimensional reconstruction. *Optik* 73:146–156.
17. Reinisch KM, Nibert ML, Harrison SC (2000) Structure of the reovirus core at 3.6 Å resolution. *Nature* 404:960–967.
18. Tang J, *et al.* (2005) The structural basis of recognition and removal of cellular mRNA 7-methyl G 'caps' by a viral capsid protein: A unique viral response to host defense. *J Mol Recognit* 18:158–168.
19. Grimes JM, *et al.* (1998) The atomic structure of the bluetongue virus core. *Nature* 395:470–478.
20. Castón JR, *et al.* (1997) Structure of L-A virus: A specialized compartment for the transcription and replication of double-stranded RNA. *J Cell Biol* 138:975–985.
21. Huiskonen JT, *et al.* (2006) Structure of the bacteriophage ϕ6 nucleocapsid suggests a mechanism for sequential RNA packaging. *Structure* 14:1039–1048.
22. Ochoa WF, *et al.* (2008) Partitivirus structure reveals a 120-subunit, helix-rich capsid with distinctive surface arches formed by quasisymmetric coat-protein dimers. *Structure* 16:776–786.
23. Cheng RH, *et al.* (1994) Fungal virus capsids, cytoplasmic compartments for the replication of double-stranded RNA, formed as icosahedral shells of asymmetric gag dimers. *J Mol Biol* 244:255–258.
24. Castón JR, *et al.* (2006) Three-dimensional structure and stoichiometry of *Helminthosporium victoriae* 190S totivirus. *Virology* 347:323–332.
25. Dryden KA, *et al.* (1993) Early steps in reovirus infection are associated with dramatic changes in supramolecular structure and protein conformation. *J Cell Biol* 122:1023–1041.
26. Chappell JD, Prota AE, Dermody TS, Stehle T (2002) Crystal structure of reovirus attachment protein σ1 reveals evolutionary relationship to adenovirus fiber. *EMBO J* 21:1–11.
27. Bassel-Duby R, *et al.* (1985) Sequence of reovirus haemagglutinin predicts a coiled-coil structure. *Nature* 315:421–423.
28. Johnson KN, Tang L, Johnson JE, Ball LA (2004) Heterologous RNA encapsidated in Pariacoto virus-like particles forms a dodecahedral cage similar to genomic RNA in wild-type virions. *J Virol* 78:11371–11378.
29. Tihova M, *et al.* (2004) Nodavirus coat protein imposes dodecahedral RNA structure independent of nucleotide sequence and length. *J Virol* 78:2897–2905.
30. Lawton JA, Estes MK, Prasad BVV (1997) Three-dimensional visualization of mRNA release from actively transcribing rotavirus particles. *Nat Struct Biol* 4:118–121.
31. Chandran K, Nibert ML (2003) Animal cell invasion by a large nonenveloped virus: Reovirus delivers the goods. *Trends Microbiol* 11:374–382.
32. Baker TS, Olson NH, Fuller SD (1999) Adding the third dimension to virus life cycles: Three-dimensional reconstruction of icosahedral viruses from cryo-electron micrographs. *Microbiol Molec Biol Rev* 63:862–922.
33. Yan X, Sinkovits RS, Baker TS (2007) AUTO3DEM—an automated and high throughput program for image reconstruction of icosahedral particles. *J Struct Biol* 157:73–82.
34. Frank J (1996) *Three-Dimensional Electron Microscopy of Macromolecular Assemblies.* (Academic, San Diego), pp 12–53.
35. Bowman VD, *et al.* (2002) An antibody to the putative aphid recognition site on cucumber mosaic virus recognizes pentons but not hexons. *J Virol* 76:12250–12258.
36. Goddard TD, Huang CC, Ferrin TE (2007) Visualizing density maps with UCSF Chimera. *J Struct Biol* 157:281–287.